Cyclostationary Signals in Battlefield Acoustics

Harry L. Hurd
Harry L. Hurd Assoc., Inc.
309 Moss Run
Raleigh, NC 27614
Tel. 919-846-9227
hurd@stat.unc.edu

September 4, 1999

Abstract

Cyclostationary signals are found when randomness occurs together with periodicity in a physical system. In this presentation we will show evidence of cyclostationarity in battlefield acoustic signals using algorithms that have been developed in the past 10 years. Cyclostationary signal processing may provide features that will aid in target classification and association.

1 Introduction

We begin with a review of the definition of cyclostationarity. Our emphasis will be discrete time processes (or sequences), indexed on $\mathbf{Z}$ but there are corresponding ideas in continuous time. A stochastic sequence $\{X(t)\}$ for $t \in \mathbf{Z}$, is said to be *cyclostationary* with period T if T is the smallest positive integer for which the mean function (of time) satisfies

$$\mu(t) = E\{X(t)\} = \mu(t+T) \tag{1}$$

and the covariance function satisfies

$$R(s,t) = E\{[X(s) - \mu(s)]\overline{[X(t) - \mu(t)]}\} = R(s+T, t+T) \tag{2}$$

for every $s, t \in \mathbf{Z}$. Observe that *stationary* processes are *cyclostationary* with every period because $R(s+T, t+T) = r(t+T-s-T) = R(s,t)$ for every s, t. Periodic functions $f(t) = f(t+T)$ are also cyclostationary because $\mu(t) = f(t)$ and $R(s,t) = f(s)\overline{f(t)}$. These are the simplest two examples. But more interesting "mixtures" of periodicity and randomness also produce cyclostationarity, as may be seen from the following examples.

Periodically modulated stationary noise. To see the cyclostationarity, suppose $Y(t)$ is a stationary random process and $f(t)$ is a periodic function, then

$$X(t) = f(t)Y(t) \tag{3}$$

is cyclostationary because $\mu_X(t) = f(t)\mu_Y$ and

$$R_X(s,t) = f(s)\overline{f(t)}R_Y(t-s) = R_X(s+T, t+T).$$

Report Documentation Page

Report Date	Report Type	Dates Covered (from... to)
04 Sep 1999	N/A	-

Title and Subtitle Cyclostationary Signals in Battlefield Acoustics	**Contract Number**
	Grant Number
	Program Element Number
Author(s)	**Project Number**
	Task Number
	Work Unit Number
Performing Organization Name(s) and Address(es) Harry L. Hurd Assoc., Inc. 309 Moss Run Raleigh, NC 27614	**Performing Organization Report Number**
Sponsoring/Monitoring Agency Name(s) and Address(es) Department of the Army, CECOM RDEC Night Vision & Electronic Sensors Directorate AMSEL-RD-NV-D 10221 Burbeck Road Ft. Belvoir, VA 22060-5806	**Sponsor/Monitor's Acronym(s)**
	Sponsor/Monitor's Report Number(s)

Distribution/Availability Statement
Approved for public release, distribution unlimited

Supplementary Notes
See also ADM201471, Papers from the Meeting of the MSS Specialty Group on Battlefield Acoustic and Seismic Sensing, Magnetic and Electric Field Sensors (2001) Held in Applied Physics Lab, Johns Hopkins Univ, Laurel, MD. on 24-26 Oct. 2001. Volume 2 (Also includes 1999 and 2000 Meetings)

Abstract

Subject Terms

Report Classification unclassified	**Classification of this page** unclassified
Classification of Abstract unclassified	**Limitation of Abstract** UU

Number of Pages
15

It can be shown that every cyclostationary process can be represented as a linear combination of periodically modulated jointly stationary processes. That is, every cyclostationary sequence can be written as

$$X(t) = \sum_{j=1}^{N} f_j(t) Y_j(t) \tag{4}$$

where the processes in the collection $\{Y_j(t), j = 1, 2, ..., N\}$ are jointly wide sense stationary and the scalar functions $f_j(t) = f_j(t+T)$ are all periodic with period T.

Phase modulated stationary noise. As above, suppose $Y(t)$ is a stationary random process and $f(t)$ is a periodic function, then

$$X(t) = Y(t + f(t))$$

is cyclostationary because $\mu_X(t) = \mu_Y$ (Y is stationary) and

$$R_X(s,t) \quad R_Y(t + f(t) - s - f(s)) = R_X(s+T, t+T).$$

Pulses with random amplitudes on a periodic schedule. This includes the communication signal format called pulse amplitude modulation (PAM) discussed by W.R. Bennett in his seminal paper on cyclostationarity[?]. If $P(t)$ is a pulse signal or function defined on the interval $[0, T)$, and A_j is a zero mean stationary sequence, then the pulse train

$$X(t) = \sum A_j P(t - jT)$$

is cyclostationary. See Bennett[?] or Gardner [?, ?] for more details.

Pulses on a periodic schedule with randomly jittered timing. This is a slight elaboration of the PAM case. Here we assume there is a zero mean stationary random (jitter) sequence δ_j for which

$$X(t) = \sum A_j P(t - jT - \delta_j).$$

Intuitively we see that $X(t)$ is cyclostationary because the stationarity of A_j and δ_j will force the distributions of $X(t)$ to be invariant under shifts of length T, provided the sum is well defined.

Stationary or white process passed through a periodically time-varying filter. If $H(t, \tau)$ $H(t+T, \tau+T)$ is the response of a periodically time varying filter at time t to an impulse at time τ, then if $Y(t)$ is stationary it may be seen from

$$X(t) \quad \sum_{u} H(t,u) Y(t-u)$$

that $X(t)$ is cyclostationary with period T. We will not elaborate.

These examples illustrate the main idea that *cyclostationary* signals are typically produced by systems in which randomness occurs together with periodicity. In the case of battlefield acoustics, we have the periodicities of engines, gears and tracks mixed together with the randomness caused by specific terrain and operating conditions. For example, for a constant velocity track vehicle the track pads will make contact or "slap" the ground at a (roughly) constant rate but the sound waves produced will differ somewhat from one slap to the next because of randomness in the terrain. This suggests a cyclostationary signal model of the PAM type. For another example, the firing rate of

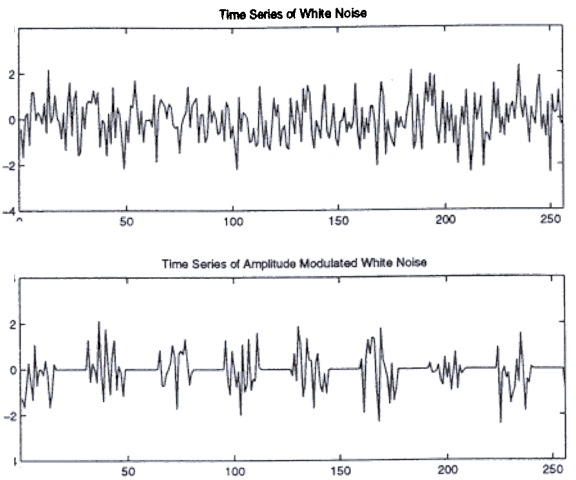

Figure 1: (Top) Simulated white noise $Y(t)$. (Bottom) Time series of $X(t) \quad f(t) \cdot Y(t)$ with $f(t) = f(t+32)$ and $f(t) = 0$ or 1 according to Eq. (5).

engines are jittered by time varying loads and governors with finite time constants. This suggests the jittered pulse train model.

In the remainder of this paper we will review some of the methods used in empirical analysis of cyclostationary signals and show some results of their application to battlefield acoustical signals.

2 Empirical Methods

The average power spectrum of a cyclostationary signal may be completely free of spectral lines, and yet the signal contains periodic structure that can be extracted. For example, in the amplitude modulation model $X(t) = f(t)Y(t)$, if $Y(t)$ has no spectral lines and $f(t)$ is not a constant, then the sample spectrum of $X(t)$ will not have any lines but still there is information about the periodic modulation in the signal. To illustrate this, suppose $Y(t)$ is white noise with variance σ_Y^2 so that $E\{Y(t)\overline{Y(t+m)}\} = \sigma_Y^2 \delta_m$. The top trace of Figure 1 presents 256 values of a simulated white sequence without amplitude modulation (a sample of $Y(t)$) and the bottom trace presents 256 values of a modulated sequence $X(t)$ for which

$$f(t) \quad \begin{cases} 1 & \text{if } 0 \leq t \leq 15 \\ a & \text{if } 16 \leq t \leq 31 \end{cases} \tag{5}$$

where $a = 0$ and $f(t+32) = f(t)$. A periodic structure is clearly seen in the bottom trace but the periodograms of Figure 2 show no perceptible evidence of periodicity at a frequency index of $j = 512/32 = 16$. The averaging of 50 independent periodograms, an operation that increases the sensitivity of determining the presence of periodic components, still shows no evidence of periodicity. Qualitatively, the periodograms of Figure 2 are identical to the periodograms of unmodulated white noise shown in Figure 3.

We now present two methods with which it is possible to extract some information about the cyclostationary structure. This information can be presented in spectrogram-like displays.

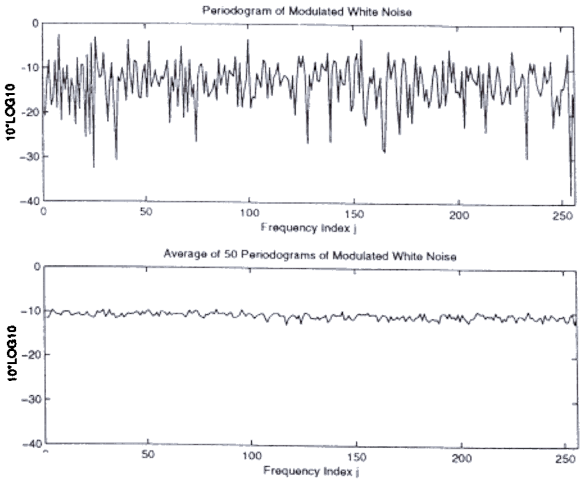

Figure 2: (Top) Periodogram of $X(t) = f(t) \cdot Y(t)$ with $f(t) = f(t+32)$ and $f(t) = 0$ or 1 according to Eq. (5). $N = 512$. The frequency corresponding to the index j is $\lambda_j = 2\pi j/N$. (Bottom) Average of 50 independent periodograms of the same series.

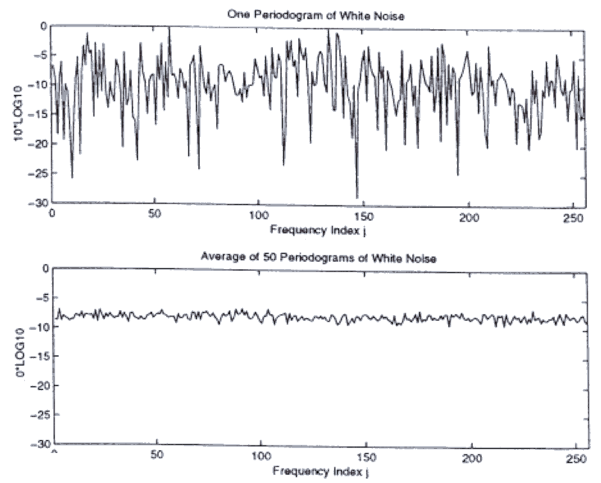

Figure 3: (Top) Periodogram of white noise $X(t)$. $N = 512$. The frequency corresponding to the index j is $\lambda_j = 2\pi j/N$. (Bottom) Average of 50 independent periodograms of the same series.

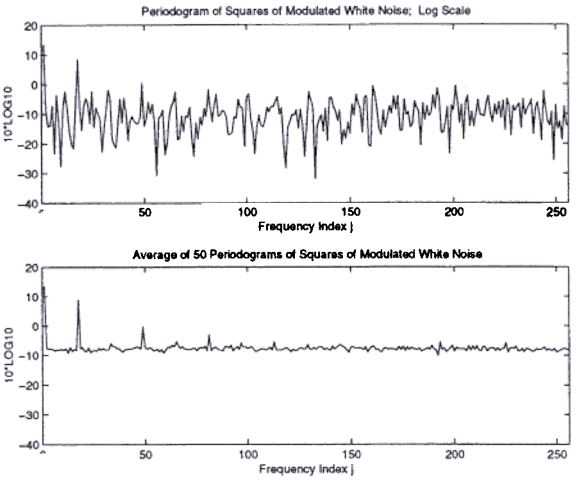

Figure 4: (Top) Periodogram of $Y^2(t)$ where $X(t) = f(t) \cdot Y(t)$ with $f(t) = f(t+32)$ and $f(t) = 0$ or 1 according to Eq. (5). $N = 512$. The frequency corresponding to the index j is $\lambda_j = 2\pi j/N$. (Bottom) Average of 50 independent periodograms of the same series.

Spectrum of the squares.

This method is very simple and can be motivated by the amplitude modulation model discussed above. The instantaneous variance of $X(t)$ is

$$\sigma_X^2(t) = |f(t)|^2 \sigma_Y^2$$

so the instantaneous variance is properly periodic (not a constant) with period T provided that $|f(t)^2|$ is properly periodic. This says that the time series of the squares $(X^2(t))$ consists of a periodic mean with additive random fluctuations about it. Since the periodogram (or spectrogram) is a well known and understood method for detecting periodicities in noise, we are thus motivated to form the periodogram of the squares of $X(t)$.

Figure 4 illustrates that the periodogram of the squares of $X(t)$ makes the periodicity very perciptible.

Can this simple modification permit us to perceive the presence of any arbitrary PC structure? The answer is no. For example, Figure 5 shows that the periodogram of the squares of $X(t) = f(t) \cdot Y(t)$ evidently shows no sign of periodicity when we take $a = -1$ in (5) for $Y(t)$ given by a first order autoregression $Y(t) = .8Y(t-1) + \epsilon(t)$, which is stationary with correlation $R_Y(k) = .8^k$. Although $X(t)$ is most certainly PC with period $T = 32$, $E\{X^2(t)\} = |f(t)|^2 R_Y(0) = R_Y(0)$ is constant with respect to t (and thus not properly periodic).

In essence, the spectrum of the squares is effective for detecting periodic amplitude modulations but a more general method is needed to look for more general cyclostationary structure. This is the topic of the next subsection.

Finally, a spectrogram-like display can be constructed from succcessive periodograms of the squared series. Examples will be presented following the next subsection.

Methods based on spectral coherence.

In order to describe a more general method of analyzing cyclostationary time series we use some spectral concepts that can be applied to some *nonstationary* processes. It is known that cyclosta-

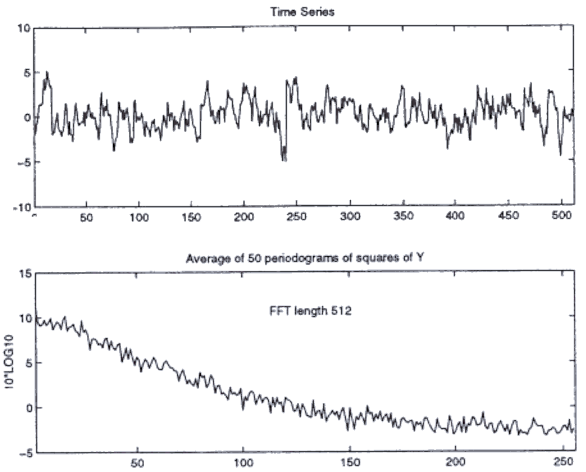

Figure 5: (Top) Time series of $Y(t) = f(t) \cdot X(t)$ with $f(t) = f(t+32)$ and $f(t) = -1$ or 1 according to Eq. (5); $X(t) = .8X(t-1)+\epsilon(t)$. $N = 512$. The frequency corresponding to the index j is $\lambda_j = 2\pi j/N$. (Bottom) Average of 50 independent periodograms of the squares of the same series.

tionary sequences are *harmonizable* (Gladyshev [2]) so

$$X(t) = \int_0^{2\pi} \tag{6}$$

where $Z($ is a random measure that does not have orthogonal increments and is related to $R(s,t)$ through

$$R(s,t) = E\{X(s)\overline{X(t)}\} = \int_0^{2\pi}\int_0^{2\pi} e^{-is\lambda_1 - it\lambda_2} r_Z\,(d\lambda_1, d\lambda_2)\,, \tag{7}$$

where the *cross spectral correlation* measure $r_Z(A,B) = E\{Z(A)\overline{Z(B)}\}$ is of bounded variation on $[0,2\pi]\times[0,2\pi]$, $\int_0^{2\pi}\int_0^{2\pi} \mid r_Z\,(d\lambda_1, d\lambda_2) \mid < +\infty$. That is, harmonizable processes still have a spectral representation (6) but the frequency amplitude process $Z(\lambda)$ need not have orthogonal increments. Although we do not prove it here, cyclostationarity forces the increment $dZ\,(\lambda_1)$ to be orthogonal to $dZ\,(\lambda_2)$ except when $\lambda_2 = \lambda_1 - 2\pi k/T$. That is, the sequence $X(t)$ is cyclostationary with period T if and only if the support of the spectral correlation measure r_Z is contained in the set $S = \bigcup_k S_k$ where $S_k = \{(\lambda_1, \lambda_2) \mid \lambda_2 = \lambda_1 - 2\pi k/T\}$. This support set is illustrated in Figure 6.

The (spectral) correlations in the increments of Z that give rise to Figure 6 is characteristic of cyclostationary sequences, and so it follows that a test (but not the only test) for the presence of cyclostationarity may be phrased in terms of a test for these specific correlations in the sample spectrum. The original idea we believe is due to N.R Goodman [3]; see Hurd and Gerr [4] for a discussion of Goodman's contribution and it's application to determining the presence of cyclostationarity in a time series. Since the sample Fourier transform may be interpreted as an estimate of the frequency increments of a harmonizable process, we first compute the finite length sample Fourier transform:

$$\hat{X}(\lambda) = \sum_{t=0}^{N-1} X(t)\exp(-i\lambda t) \tag{8}$$

where $\hat{X}(\lambda)$ is typically computed at the finite set of frequencies $\lambda_k = 2\pi k/N, k = 0,1,\ldots,N-1$ and then the random variables $Z_k = \hat{X}(2\pi k/N)$ are interpreted as estimates of $dZ(2\pi k/N), k =$

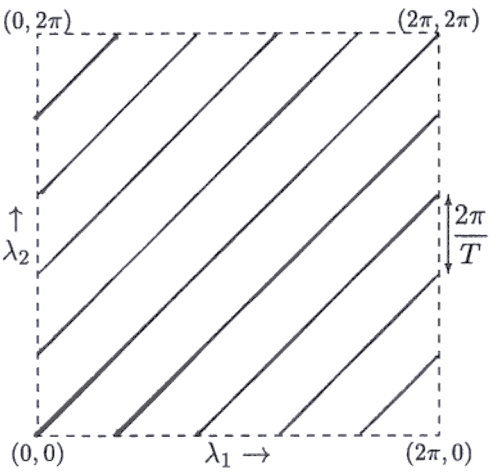

Figure 6: Support of r_Z for a cyclostationary sequence.

$0, 1, \ldots, N-1$. The spectral coherence computation determines the normalized correlation, or coherence, between two bands $Z_p, Z_{p+1}, \ldots Z_{p+M-1}$ and $Z_q, Z_{q+1}, \ldots Z_{q+M-1}$ of frequency-indexed variates where each band contains M variates indexed consecutively. Precisely, we compute

$$|\gamma(p,q,M)|^2 = \frac{|\sum_{m=0}^{M-1} Z_{p+m}\overline{Z_{q+m}}|^2}{\sum_{m=0}^{M-1}|Z_{p+m}|^2 \sum_{m=0}^{M-1}|Z_{q+m}|^2} \tag{9}$$

for (p, q) in a square array and plot the values exceeding a threshold according to a grey-scale encoding. In the univariate case, under the assumption that the Zj are i.i.d. complex Gaussian variates the null distribution for $\gamma(p,q,M)|^2$ is given by $Pr[|\gamma|^2 > |\gamma_0|^2] = (1-|\gamma_0|^2)^{M-1}$ (see [4]). A variant of this idea was the basis the test for cyclostationarity used in Bloomfield, Hurd and Lund (1994) [1].

The display of Figure 7 presents a (diagonal) spectral coherence image made from a segment of the XC5 acoustic time series in which there was a vehicle moving toward a sensor array. The periodogram of the signal, shown in the lower display, shows no evidence of periodicity but yet the periodicity in the spacing of the diagonal lines in the spectral coherence image is easily seen.

The persistence along the diagonal lines suggests the averaging of the image along lines of constant difference frequency. The result of this averaging for this image is shown in Figure 8. The periodic spacing is again clear and it's perception is enhanced (gain in signal to noise ratio). Although the summing along lines of constant difference frequency is incoherent, the coherence in the raw spectrum has already been used to form the spectral coherence image. If a sequence of these diagonal averages are computed for successive time segments, then one may make an *average-coherence gram* plot of the successive diagonal averages and hence perceive the difference frequencies of the support lines. These difference fequencies are sometimes called the cycle frequencies of the cyclostationary process. The *average-coherence spectrogram* permits the perception of even much weaker cyclostationary signals.

Sometimes, as in Figure 7, the spectral coherence may be usefully large only in some locations along a difference frequency line. Thus in computing the *average-coherence gram*, restricting the diagonal average to certain areas can further enhance the perceptibility of weak signals.

We will now present examples of the *squares spectrogram* and the *average-coherence gram* produced from battlefield acoustic time series. The main purpose here is to demonstrate the potential

Figure 8: Result of diagonal averaging applied to spectral coherence image of Figure 7. The abcissa is difference frequency (distance from the diagonal in Figure 7).

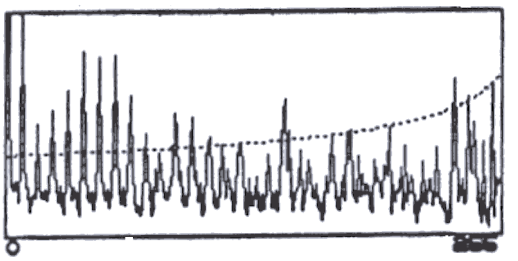

Data GV9A1060 The *usual spectrogram*of Figure 9 shows a mixture of a dynamic harmonic set along with a few straight lines. Figure 10 contains an *average coherence spectrogram*and a *squares spectrogram*. The *squares spectrogram*appears much like the *usual spectrogram*in line SNR and texture so we have concentrated on the *average coherence spectrogram*. Figure 11 shows how the *average coherence spectrogram*depends on the difference frequency search region. The search region is a rectangle in the space of bin pairs defined by a range of X bins and a range of Y bins. That is, only the spectral coherence in the rectangle **yBins** $\times$ **xBins** are used in forming the averages that produces the scans for the *average coherence spectrogram*. The displays of Figure 11 use four different frequency search regions, each representing a quarter of the frequency band from 0 to the Nyquist frequency. Thus for a 4096 point FFT, the search region for the first quarter is $[1:512] \times [1:512]$ and for the second quarter it is $[513:1024] \times [513:1024]$.

The displays of Figure 11 show the harmonic set is much more clearly defined on the *average coherence spectrogram*than on the *usual spectrogram*. This is an important indicator for cyclostationarity. If the observed bandwidth of the line on the *average coherence spectrogram*were roughly the same as on the *usual spectrogram*, then the increased coherence level could be partly attributed to signal band shape. But the narrowness of the *average coherence spectrogram*line means that only a very precisely determined difference frequency gives rise to significantly higher spectral coherences. Other observations of this phenomenon are also seen in the remaining examples.

We also observe from Figure 11 that the *average coherence spectrogram*SNR values (line darkness) are a function the search band. In addition the gram SNR in higher frequency search regions is more time dependent, suggesting range and aspect effects.

Data GV9C1069 The *usual spectrogram*of Figure 12 shows a mixture of a strong harmonic set along with a weaker harmonic set. Figure 13 shows how the "fuzziness" of the harmonic signals are much more clearly defined on the *average coherence spectrogram*. Further, the *average coherence spectrogram*for the 2nd quarter search region appears to separate the two sources (the fundamentals of the two harmonic sets), suggesting an aspect dependence for these sources. The gram SNR levels were too small in the 3rd and 4th quarter bands to warrant inclusion.

Data VGPH This data was taken from a seismic sensor. The *usual spectrogram*of Figure 14 shows a mixture of a dynamic harmonic set along with one strong straight line. The *average coherence spectrogram*and *squares spectrogram*of Figure 15 show again how the fundamental of the harmonic family become very well defined in the *average coherence spectrogram*. Also the harmonic set is essentially absent from the *squares spectrogram*, suggesting that the harmonic set results from a phase modulation phenomenon as opposed to an amplitude modulation. But still the *squares spectrograms*hows some time intervals in which strong amplitude modulations exist.

Figure 7: (Top) Spectral coherence image from XC5_7 time series. Starting time: 69,520 samples. N=8192, M=32. Frequencies shown are in the range $.003125F_s, .006238F_s$. (Bottom) Periodogram of the same data for same frequency band with N=8192.

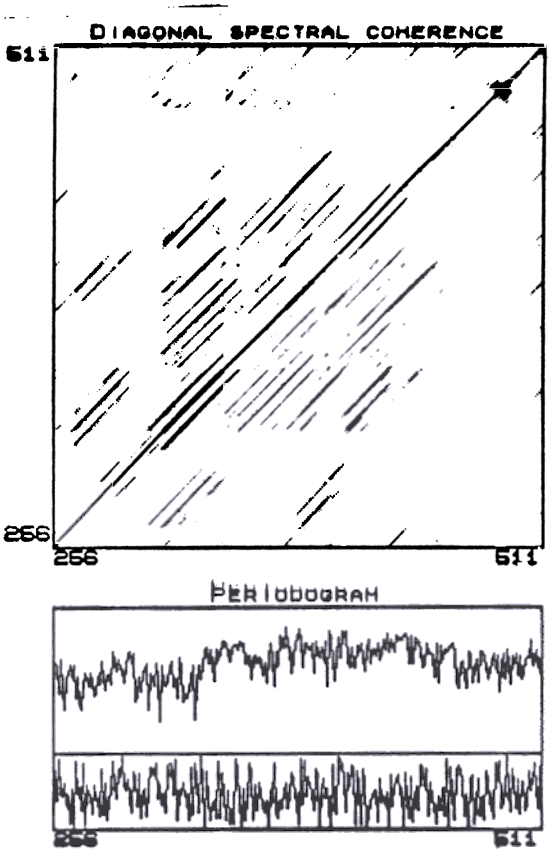

of these processing techniques and displays for contributing to the classification, detection or association of multiple acoustic targets.

3 Application to Acoustic Data

This section presents the results of analysis of several signals using the following three types of spectrograms.

The usual spectrogram, meaning a spectrogram composed of successive scans of the magnitudes of sample Fourier transforms. In some cases a *noise spectrum equalization* algorithm was employed to enhance weak lines and to equalize the spectrum for display. This algorithm was not needed for the grams based on cyclostationary processing because the algorithms tend to yield a flat background spectrum (see figure 4).

The squares spectrogram, meaning the usual spectrogram of the time series of the squares (i.e., $x^2(t)$).

The average coherence spectrogram, formed conceptually by averaging the spectral coherence image along lines of constant difference frequency.

Figure 9: Usual spectrogram of data GV9A1060; FFTLEN=2048; SLIDE=1024; NSE : ON.

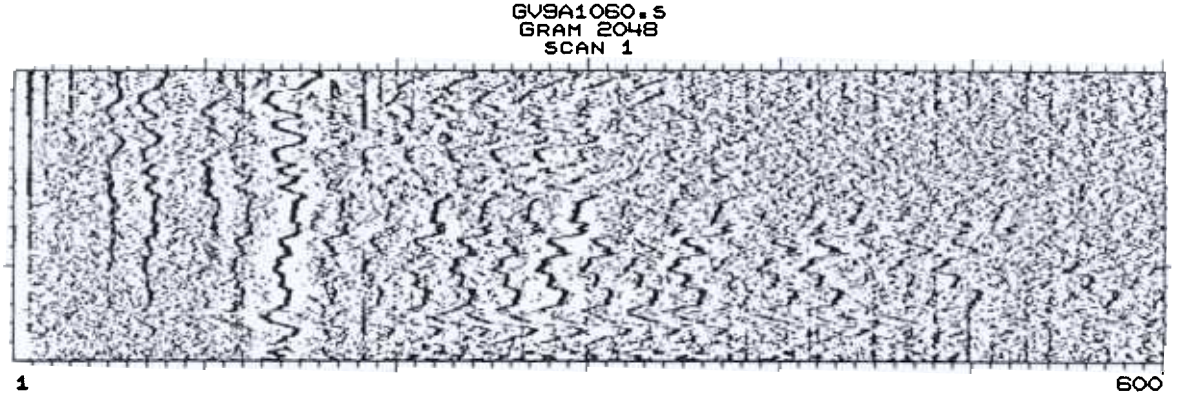

Data 20-7 This is acoustic data containing two targets. The *usual spectrogram*of Figure 16 shows a mixture of two harmonic sets along with another family of closely spaced lines suggesting a long-period modulation. Figure 17 shows *average coherence spectrograms* for the 1st and 2nd quarter search regions. The right display of Figure 17 appears to separate the two sources (the fundamentals of the two harmonic sets) in frequency and time. The time separation of the strongest portions is consistent with the time between CPAs of the two vehicles. Perhaps the most interesting new feature is the long period modulation which is evident in the left display of Figure 17. The modulation frequency is about 1 Hz.

References

[1] W. R. Bennett, "Statistics of Regenerative Digital Transmission, " *Bell System Tech. J.*, 37, pp. 1501-1542, 1958.

[2] P. Bloomfield, H. L. Hurd and R. Lund, "Periodic Correlation in Stratospheric Ozone Time Series", *J. Time Ser. Anal.*, pp. 127-150, vol. 15, No. 2, 1994.

[3] W. A. Gardner, *Introduction to Random Processes with Application to Signals and Systems*, Macmillan, New York, 1985.

[4] W. A. Gardner, *Statistical Spectral Analysis: A Nonprobabilistic Theory*, Prentice Hall, Englewood Cliffs, NJ, 1987.

[5] E. G. Gladyshev, "Periodically Correlated Random Sequences," *Sov. Math.*, vol. 2, pp. 385-388, 1961.

[6] N. R. Goodman, "Statistical Tests for Nonstationarity within the Framework of Harmonizable Processes," Rocketdyne Research Report No. 65-28, AD619270, August 2, 1965.

[7] H. L. Hurd and N. L. Gerr, "Graphical Methods for Determining the Presence of Periodic Correlation in Time Series," *J. Time Series Anal.*, vol. 12, No. 4, pp. 337-350, 1991.

Figure 10: (Left) Average coherence gram of data GV9A1060; FFTLEN=2048; SLIDE=1024; `xBins=[513:1024], yBins=[513:1024]`. (Right) Squares spectrogram of data GV9A1060; FFTLEN=2048; SLIDE=1024.

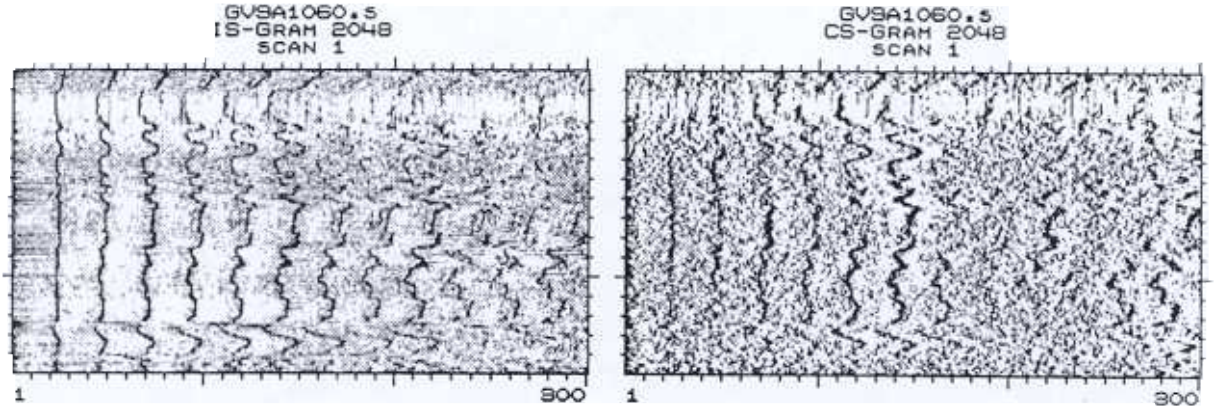

Figure 11: Average coherence grams of data GV9A1060; FFTLEN=2048; SLIDE=1024. (Top left) `xBins=[1:512], yBins=[1:512]`.
(Top right) `xBins=[513:1024], yBins=[513:1024]`.
(Bottom left) `xBins=[1025:1536], yBins=[1025:1536]`.
(Bottom right)`xBins=[1537:2048], yBins=[1537:2048]`.

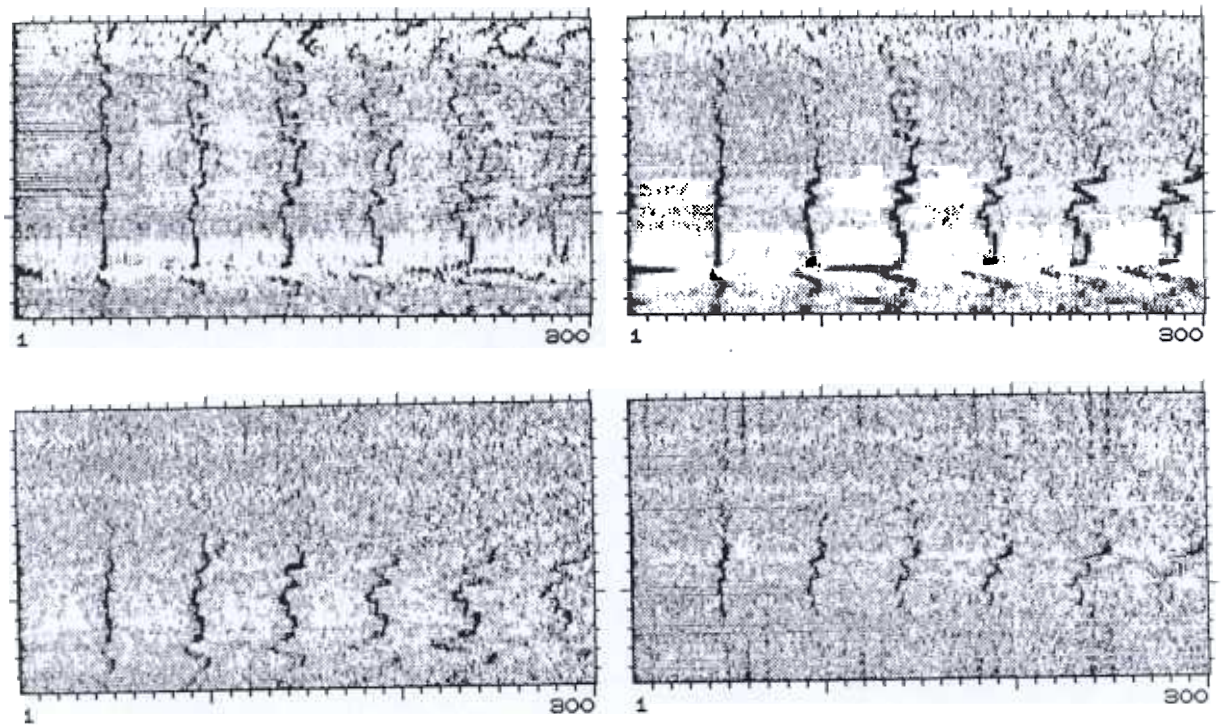

Figure 12: Usual spectrogram of data GV9C1069; FFTLEN=4096; SLIDE=1024; NSE : ON.

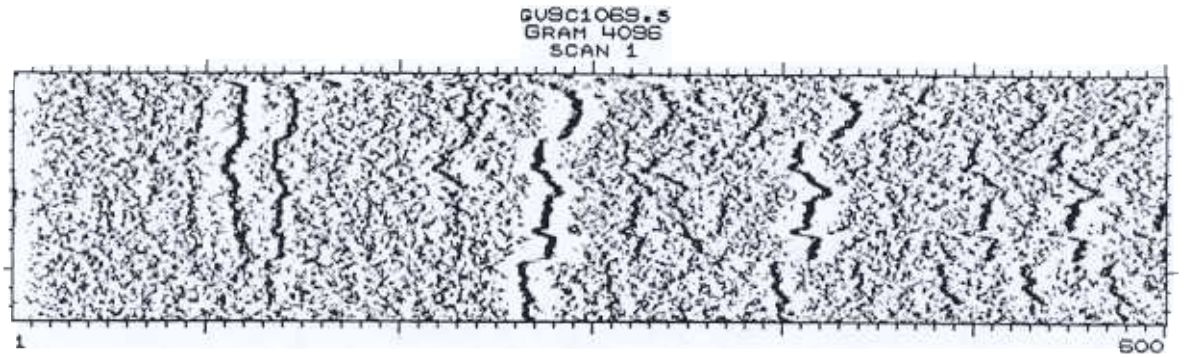

Figure 13: Average coherence grams of data GV9C1069; FFTLEN=4096; SLIDE=1024. (Left) `xBins=[1:512], yBins=[1:512].` (Right) `xBins=[513:1024], yBins=[513:1024].`

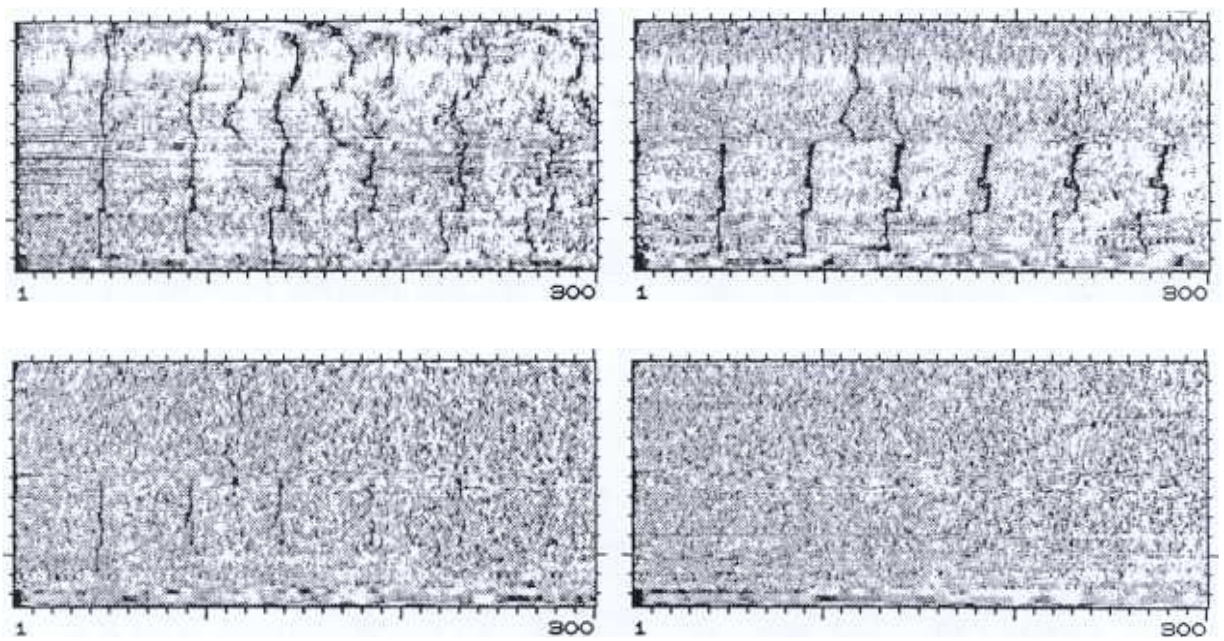

Figure 14: Usual spectrogram of data VGPH. FFTLEN=4096; SLIDE=512; NSE : ON; (Top) BAND : [1:512]; (Bottom) BAND : [1:512].

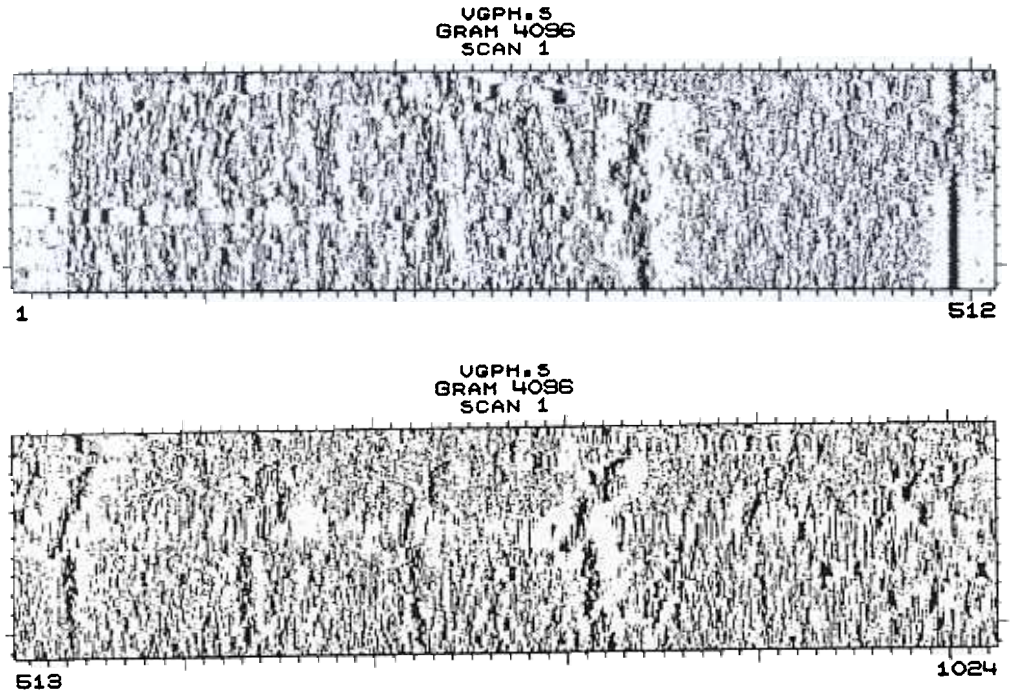

Figure 15: (Left) Average coherence gram of data VGPH; FFTLEN=4096; SLIDE=512; `xBins=[513:1024], yBins=[513:1024]`. (Right) Squares spectrogram of data VGPH; FFTLEN=4096; SLIDE=512.

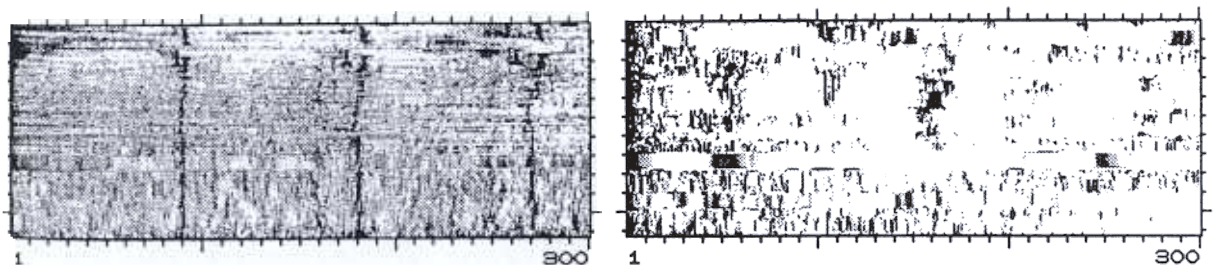

Figure 16: Usual spectrogram of data 20-7; FFTLEN=8192; SLIDE=1024; NSE : ON.

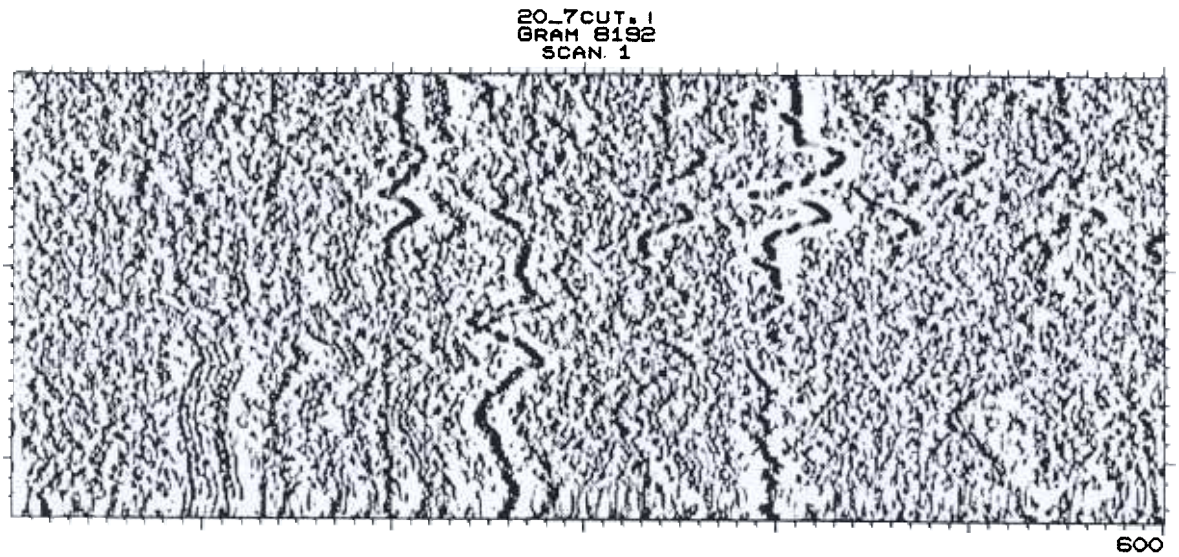

Figure 17: Average coherence grams of data 20-7; FFTLEN=8192; SLIDE=1024.
(Left) `xBins=[1:1024], yBins=[1:1024].`
(Right) `xBins=[1025:2048], yBins=[1025:2048].`